Proceedings of the 1999 IEEE
International Conference on Robotics & Automation
Detroit, Michigan • May 1999

Hybrid Micro-Gravity Simulator Consisting of a High-Speed Parallel Robot

Toshifumi Akima*, Susumu Tarao** *and* Masaru Uchiyama*

*Graduate School of Engineering, Tohoku University
Aoba-yama 01, Sendai 980-8579, Japan
**Ichinoseki National College of Technology
Takanashi, Hagisyou, Ichinoseki 021-8511, Japan

Abstract

In ground testing of a spacecraft system, a simulator system which emulates a micro-gravity environment is necessary. It is demanded that the simulator system has wide response frequency bandwidth when it deals with motions having contacts and collisions. The authors have been developing a hybrid micro-gravity simulator which has wide response bandwidth. Its motion table is a high-speed parallel robot driven by powerful direct drive motors. In preliminary experiments, this robot has achieved accelerations up to 40 [G]. In this paper, we report an outline of the simulator and discuss the obtained experimental results.

1 Introduction

Space robotics technology and rendezvous-docking technology are the indispensable ones in space developments in recent years. Though it is necessary to analyze these technologies theoretically, suitable hardware applying these technologies must also be developed. Developing hardware demands efficient ground testing and hence we come across a demand for the necessary testing equipment. In addition, the ground equipment is also necessary in order to establish new control laws for space robots and docking techniques. Though it is difficult, a micro-gravity environment in the orbit must be emulated on ground in such experiments. One of the emulation methods for the micro-gravity environment is introduced in [1]. It is a hybrid micro-gravity simulator which loads the devices (e.g. sensors, actuators) to be evaluated onto a motion table consisting of suitable servo mechanisms.

There are some research reports found related to this hybrid simulator. Shimoji et al. developed the hybrid simulators which emulated capturing and berthing of a floating object [2] [3]. These simulators used real hardware to capture a target and a servo mechanism to realize the floating object motion.

Different docking simulators have been developed by Grimbert [4] [5] and Inoue [6]. Loading the docking mechanism of the simulated spacecraft onto a servo mechanism, these simulators emulate the relative motion between the two spacecraft in space.

Dubowsky et al. developed the VES (Vehicle Emulation System) that is a widely used simulator system which can emulate motions for any objects [7] [8]. This system can emulate various objects (e.g. a floating object, elastic beam in micro-gravity environment) by varying the computational models.

Response frequency bandwidth for all these hybrid simulators is more or less about 10 [Hz]. It was possible for the bandwidth of these simulators to emulate objects precisely because they dealt with the systems whose natural frequencies were only a few hertz. But whether these simulators could emulate the high-speed dynamics which could appear in impacts like collisions is not known.

For this problem, using the VES, Yoshida et al. simulated the impact dynamics of spaceborne manipulator systems [9]. In their simulator system, a real manipulator was used as a device to deal with the impulsive motion, and a servo mechanism was used as a device to deal with the low frequency motion of flexible base. This is an effective method to simulate the impulsive motion of a manipulator fixed on a slowly movable base.

On the other hands, we will be able to find another approach to simulating impulsive motion, if the limits of response frequency bandwidth for the hybrid simulators can be improved.

Therefore, the objective of this research is to develop a hybrid micro-gravity simulator, which can emulate the impulsive motions, consisting of a high-speed parallel robot as its motion table and to evaluate its response frequency bandwidth.

0-7803-5180-0-5/99 $10.00 © 1999 IEEE

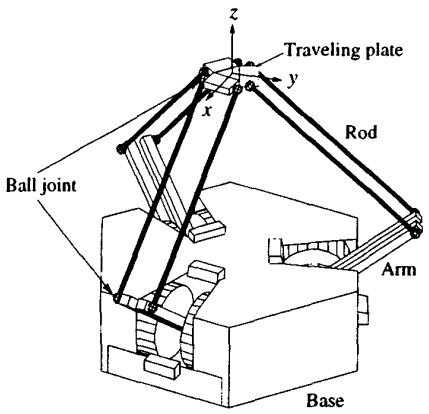

Figure 1: Schematic view of HEXA97 robot.

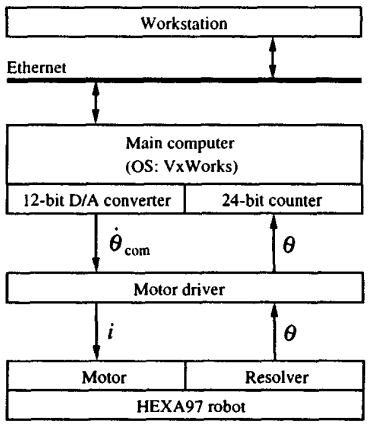

Figure 2: Control system of HEXA97 robot.

2 High-speed parallel robot

2.1 HEXA parallel mechanism

A schematic view of a high-speed parallel robot consisting of the HEXA mechanism (hereinafter called, HEXA97 robot) is shown in Figure 1. HEXA97 robot is facing up on the frame which has a three-pillar. This robot is driven by six direct drive motors which are paired and facing each other. In HEXA mechanism, since all heavy actuators are placed in the fixed base, it is possible to make the movable parts very light. High-speed action is possible also for this reason. The arms which are first links are fixed through flanges on each motor. The rods which are second links are connected to arms through ball joints. The traveling plate which is the end link is connected to rods in the same way.

2.2 Control system

The control system of HEXA97 robot is shown in Figure 2. The main computer uses PC/AT compatible machine (CPU: MMX Pentium 233 [MHz]) and VxWorks which is a real-time OS. The rotation angle of a motor is detected by a resolver built in the motor. The analog signal output from the resolver is fed into the motor driver. It is converted in a digital signal which is utilized in the velocity feedback loop. The motor driver outputs a pulse train signal which is taken into the main computer through a pulse counter board. The main computer calculates controlled variable following a given control law and outputs a velocity command to the motor driver through a D/A converter.

As a control law, PD control with velocity feedforward and gravity compensation is adopted. While the gravity compensation torque is calculated based on a simple model as mentioned in subsection 2.4, it is able to improve the accuracy of path tracking. Block diagram of this control law is given in Figure 3. Velocity command to motors is represented by

$$\dot{\boldsymbol{\theta}}_{\mathrm{com}} = K_{\mathrm{v}}^{-1}\boldsymbol{\tau}_g + \dot{\boldsymbol{\theta}}_{\mathrm{d}} + K_{\mathrm{p}}\left(\boldsymbol{\theta}_{\mathrm{d}} - \boldsymbol{\theta}\right) + K_{\mathrm{d}}\left(\dot{\boldsymbol{\theta}}_{\mathrm{d}} - \dot{\boldsymbol{\theta}}\right), \quad (1)$$

where

K_{v} = proportional gain of velocity servo loop,
$\boldsymbol{\tau}_g$ = gravity compensation torque.

A desired motor angle and angular velocity are calculated by the inverse kinematics using desired traveling plate trajectory. Velocity servo loop in the motor driver realizes a software servo at a sampling frequency of 1.8 [kHz]. Sampling frequency of the main position servo feedback loop is about 1.0 [kHz]. PD control gains are $K_{\mathrm{p}} = 150$ [s^{-1}] and $K_{\mathrm{d}} = 3.0$, respectively.

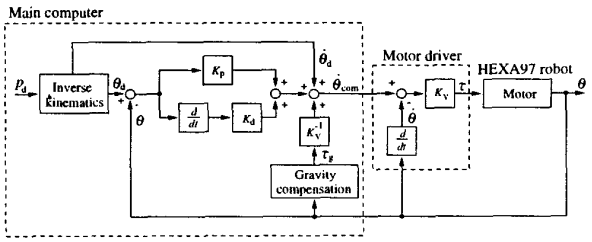

Figure 3: Block diagram of the control law.

2.3 Inverse and forward kinematics

The inverse kinematics and forward kinematics of the HEXA mechanism is described in this subsection. In general, it is easy to solve a parallel robot inverse kinematics analytically, and the solution of the HEXA mechanism inverse kinematics is available in [10]. On the other hand it is generally difficult to solve a parallel robot forward kinematics analytically. In order to calculate the gravity compensation torque mentioned next subsection, the position and the attitude of the traveling plate are necessary. They can be known by the forward kinematics calculation using the motor rotation angles. Hence, an iterative method is used for HEXA97 robot in order to calculate the numerical solution of forward kinematics using Jacobian matrix. The algorithm for the method is:

Step 1: Joint angle vector $\boldsymbol{\theta}_0$ is given. Initialize $i = 1$, and a suitable traveling plate position and attitude vector $\boldsymbol{p}_i$ is decided.

Step 2: Calculate $\boldsymbol{\theta}_i$ corresponding to $\boldsymbol{p}_i$ by the inverse kinematics.

Step 3: Calculate Jacobian matrix $\boldsymbol{J}$.

Step 4: For error $\boldsymbol{\theta}_0 - \boldsymbol{\theta}_i$, decide $\boldsymbol{p}_{i+1}$ by the following equation:

$$\boldsymbol{p}_{i+1} := \boldsymbol{p}_i - \boldsymbol{J}\,(\boldsymbol{\theta}_0 - \boldsymbol{\theta}_i).$$

Step 5: Set $i := i + 1$.

Step 6: Repeat from Step 2 to Step 5. If error $\boldsymbol{\theta}_0 - \boldsymbol{\theta}_i$ becomes small enough, the corresponding $\boldsymbol{p}_i$ is taken as $\boldsymbol{p}_0$.

2.4 Gravity compensation

Gravity compensation torque is calculated based on a simple model of HEXA97 robot shown in Figure 4. In this model, the rod has been assumed as a stick of zero mass and zero moment of inertia. The actual mass of rod is distributed onto the respective arm and the traveling plate equally. In other words, a virtual arm and a virtual traveling plate can be defined. The virtual traveling plate includes the load (e.g. force/torque sensor and real model object presented in subsection 3.1), in case of the load is on the plate. Then the gravity compensation torque consists of a term corresponding to the virtual traveling plate and one to the virtual arm, and can be written as

$$\boldsymbol{\tau}_{\mathrm{g}} = \boldsymbol{\tau}_{\mathrm{vt}} + \boldsymbol{\tau}_{\mathrm{va}}. \tag{2}$$

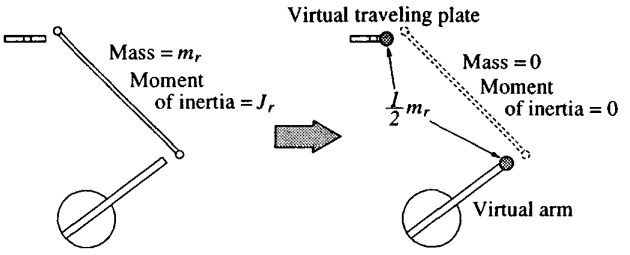

Figure 4: A simple model of HEXA97 robot.

The virtual traveling plate term is

$$\boldsymbol{\tau}_{\mathrm{vt}} = \boldsymbol{J}^T \boldsymbol{G}(\boldsymbol{p}), \tag{3}$$

where $\boldsymbol{J}$ is Jacobian matrix, $\boldsymbol{G}(\boldsymbol{p})$ is force/moment vector due to gravity acting on center of gravity of the virtual traveling plate.

$$\boldsymbol{G}(\boldsymbol{p}) = \begin{bmatrix} M_{\mathrm{vt}}\,\boldsymbol{g} \\ M_{\mathrm{vt}}\overrightarrow{O_t G_{\mathrm{vt}}} \times \boldsymbol{g} \end{bmatrix}, \tag{4}$$

where

M_{vt} = virtual traveling plate mass [kg],
G_{vt} = virtual traveling plate CG in Σ_t (a frame fixed on the traveling plate), and
$\boldsymbol{g}$ = gravity acceleration vector ($\boldsymbol{g} = [\ 0 \quad 0 \quad -g\ ]^T$ [m/s^2]).

The virtual arm term is

$$\boldsymbol{\tau}_{\mathrm{va}} = -L_{G\mathrm{va}} M_{\mathrm{va}} g \cos\theta, \tag{5}$$

where

$L_{G\mathrm{va}}$ = shortest distance from the motor axis to the virtual arm CG [m]
M_{va} = virtual arm mass [kg]
θ = motor rotation angle [rad].

2.5 Fast motion experiment

A preliminary experiment was performed in order to investigate maximum velocity and acceleration of HEXA97 robot.

Keeping the attitude of the traveling plate as (0.0, 0.0, 0.0) [rad], it is moved from (0.0, 0.0, 0.23) [m] to (0.0, 0.0, 0.80) [m] and then down to (0.0, 0.0, 0.30) [m] in Σ_b (a reference frame fixed on the base). A trajectory was generated by 4-1-4 polynomial interpolation. Experimental results are shown in Figures 5.

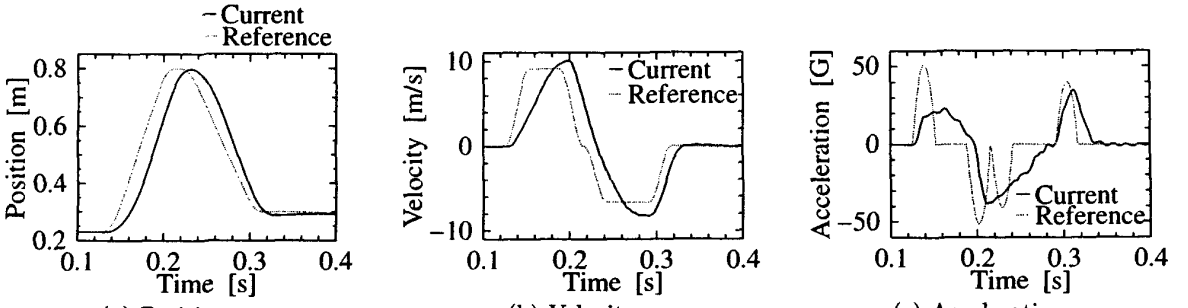

(a) Position. (b) Velocity. (c) Acceleration.

Figure 5: Experimental results.

It is clear that HEXA97 robot achieved maximum velocity of 10 [m/s] and maximum acceleration of 40 [G] at traveling plate center. These results show that simulation of high-velocity and high-acceleration motion is possible for the micro-gravity simulator consisting of HEXA97 robot.

3 Hybrid micro-gravity simulator

It is necessary to emulate a micro-gravity environment in the orbit to ground testing of a spacecraft system. The micro-gravity environment can be realized in the following ways: free-fall in a drop tower or ballistic flight, utilizing buoyancy of water and utilizing air-bearings. However, there are various problems with these methods specially related to length of experimental time and opportunity of availability. Moreover, experimental conditions are also limited and hence it is difficult to get dynamic accuracy. Due to these problems, a hybrid micro-gravity simulator, like one described in this paper, is adopted.

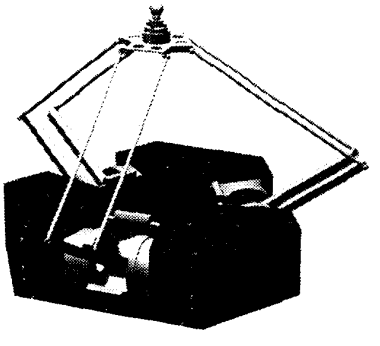

Figure 6: A schematic view of a hybrid micro-gravity simulator realized with HEXA97 robot.

3.1 Simulator system

A schematic view of a hybrid micro-gravity simulator consisting of HEXA97 robot is shown in Figure 6. A force/torque sensor and a part of the object whose response is to be simulated (hereinafter called, real model) are attached to the traveling plate. The rest of the parts of the object (hereinafter called, virtual model) are put in a main computer as their dynamic models. Using the hybrid model, which is combination of the real model and the virtual model, the motions of a spacecraft in the orbit can be realized.

External forces that act on the real model can be measured by the force/torque sensor. These forces are input to the virtual model in the computer. Dynamic simulation is performed following equations of motion of the virtual model. The motion of the virtual model is computed corresponding to the input data from the force/torque sensor. Motions of the simulated object in the micro-gravity environment are realized by tracking HEXA97 robot to these computed result. A scheme of these computations is shown in Figure 7.

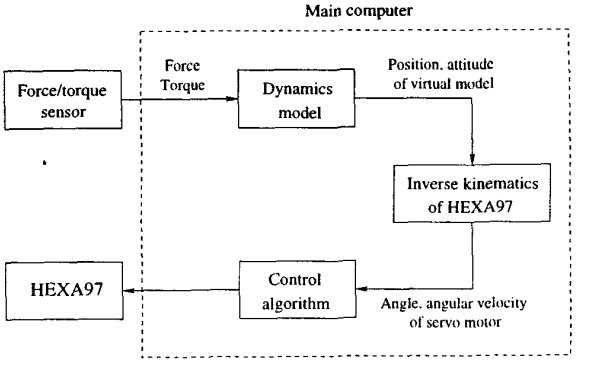

Figure 7: Block diagram of simulator.

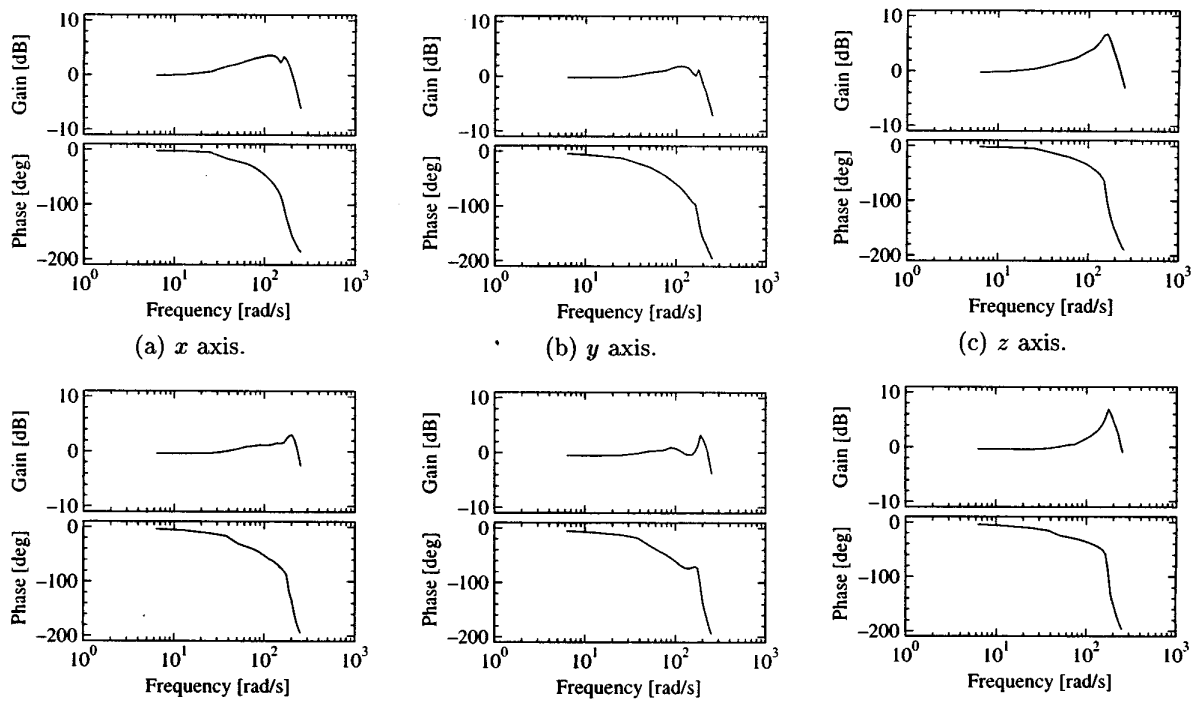

(a) x axis. (b) y axis. (c) z axis.

(d) Around x axis. (e) Around y axis. (f) Around z axis.

Figure 8: Bode plots.

3.2 Frequency response experiment

To estimate the response bandwidth of the simulator, frequency response experiments were performed.

A hybrid micro-gravity simulator has a limitation of response frequency bandwidth due to its working principal. It is caused due to computational time-delay of dynamic simulation of the virtual model and a delay of the servo mechanism. After a force is detected, there exists a certain delay until appearance of the motions caused by that force. Hence it is necessary to evaluate the response bandwidth of the simulator. Response bandwidth can be estimated from frequency response of HEXA97 robot itself when it is working in the simulator system. The amplitude of the input sine wave must be set appropriately to get a better response. It should be such that it may not cause saturation of the motor torques and hence collisions of the simulated spacecraft with external objects. In general, during contacts and collisions, some assumptions are made. Interaction forces are high and impulsive, and its duration are very short. Furthermore the velocity changes are nearly instantaneous and the changes in position and orientation of objects are negligible. Hence, it is considered that the impulsive motions which are caused by contacts and collisions have high frequencies but low amplitudes. Therefore, considering these low amplitude vibrations, we select here an amplitude of 0.005 [m] for translational vibrations and 3 [deg] for rotational ones, respectively. The amplitude of the rotational motion is the same amplitude as that for translational one in the motor angular space. The input is a sine trajectory of the traveling plate center. The output is the trajectory of the same point that is computed by forward kinematics using the motor angles. At first the traveling plate center is moved to (0.0, 0.0, 0.5) [m] in Σ_b. Then the sine trajectory in the desired direction is input to HEXA97 robot. For translational motion, the average of the sine trajectory is at (0.0, 0.0, 0.5) [m], and that for rotation of the traveling plate is at zero of the rotational motion. Frequency of the input is varied as 1 [Hz], 2 [Hz] up to 40 [Hz] with a step of 2 [Hz].

The basic experimental results with no load on the traveling plate are shown in Figure 8. Bode plots show a resonance point at about 160 [rad/s]. HEXA97 robot has a bandwidth of 260 [rad/s] at this input amplitude. The shapes of Bode plots are different from one another, because loading of motors varies due to the arrangement of motors during motions along each direction or around each axis. There are two resonance points in each motion except in the z-axis direction

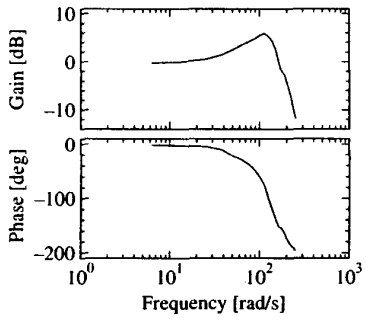

(a) z axis.

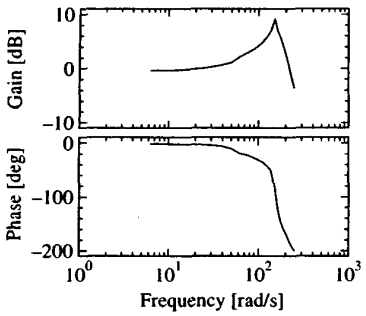

(b) Around z axis.

Figure 9: Bode plots with load on the plate.

and around z-axis. It is considered that lower resonance point is controller's one and higher one is due to the resonance of rods. This can be shown that the first bending mode of rods matches with the higher resonance point in the above Bode plots.

Next, in the z-axis direction and around z-axis, the experimental results with loads: a force/torque sensor and a real model on the traveling plate are shown in Figure 9. Each mass of the force/torque sensor and the real model is 0.710 [kg] and 0.288 [kg]. Though suffered response loss from the load on the traveling plate, HEXA97 robot with loads has a bandwidth of 200 [rad/s] at this input amplitude. This is almost the same in the other motions: along x-axis or y-axis direction and around x-axis or y-axis.

From the obtained Bode plots, it is considered that a little improvement of the control gains and increasing the stiffness of rods is needed. However, it can be concluded that the HEXA97 robot can emulate high velocity and high acceleration motions in micro-gravity environment.

4 Conclusion

In this paper, the concept of a hybrid micro-gravity simulator consisting of HEXA97 robot as its motion table is mentioned. Some preliminary experiments and frequency-response plots of HEXA97 robot itself are given to evaluate the performance of the simulator. In the future work, an object to be simulated will be chosen and the simulator will be constructed actually. It is hoped to select a model of a spacecraft to be simulated in the micro-gravity environment.

References

[1] K. Yoshida, "Experimental Platforms for Research and Development of Space Robots," *Journal of the Robotics Society of Japan*, vol. 14, no. 1, pp. 18–21, 1996. (in Japanese)

[2] H. Shimoji et al., "Simulation System for a Space Robot Using 6 Axis Servos," *Proc. of XIth IFAC Symposium on Automatic Control in Aerospace*, pp. 131–136, 1989.

[3] H. Shimoji et al., "Evaluation of Space Robot Behavior Using Berthing Dynamics Simulator," *Journal of the Robotics Society of Japan*, vol. 13, no. 1, pp. 127–133, 1995. (in Japanese)

[4] D. Grimbert et al., "DYNAMIC TESTING OF A DOCKING SYSTEM," *Proc. 1st European In-Orbit Operations Technology Symposium*, ESA SP-272, pp. 281–288, 1987.

[5] D. Grimbert et al., "DDTF IMPROVEMENT FOR MORE ACCURATE SPACE DOCKING SIMULATION," *Proc. 2nd European In-Orbit Operations Technology Symposium*, ESA SP-297, pp. 239–244, 1989.

[6] M. Inoue et al., "Development of the Docking Dynamics Simulator," *Trans. of SICE*, vol. 28, no. 11, pp. 1306–1313, 1992. (in Japanese)

[7] S. Dubowsky et al., "A Laboratory Test Bed for Space Robotics: The VES II," *Proc. of IEEE/RSJ Int. Symp. on Intelligent Robot System (IROS'94)*, Munich, Germany, pp. 1562–1569, 1994.

[8] T. Corrigan, "The Development and Application of Methods for Emulating Micro-Gravity," S.M. Thesis, Department of Mechanical Engineering, MIT, Cambridge, MA, May 1994.

[9] K. Yoshida et al., "Experimental Results on Impact Dynamics of Spaceborne Manipulator Systems," *Proc. of the 4th Int. Symp. on Experimental Robotics, Lecture Notes in Control and Information Science*, pp. 436–447, 1995.

[10] F. Pierrot et al., "A New Design of a 6-DOF Parallel Robot," *Journal of Robotics and Mechatronics*, vol. 2, no. 4, pp. 308–315, 1990.